Electronic Supporting Information

Anomalously-low activation energy of nanoconfined $MgCO_3$ precipitation

Quin R.S. Miller [ab], John P. Kaszuba [ac], Herbert T. Schaef [b], Mark E. Bowden [d], B. Peter McGrail [e], and Kevin M. Rosso [b]*

[a] Department of Geology and Geophysics, 1000 E. University Avenue, University of Wyoming, Laramie, WY 82071, USA

[b] Physical and Computational Sciences Directorate, Pacific Northwest National Laboratory, P. O. Box 999, MS K8-98, Richland, WA 99352, USA

[c] School of Energy Resources, 1000 E. University Avenue, University of Wyoming, Laramie, WY 82071, USA

[d] William R. Wiley Environmental Molecular Sciences Laboratory, Pacific Northwest National Laboratory, P. O. Box 999, MS K8-98, Richland, WA 99352, USA

[e] Energy and Environment Directorate, Pacific Northwest National Laboratory, P. O. Box 999, MS K8-98, Richland, WA 99352, USA

[*] Corresponding author contact information: quinrs.miller@pnnl.gov

Materials

High-surface area (26.7±0.1 m^2/g) synthetic forsterite powder, previously described by Miller et al. [1-2], was used in this study. The forsterite, which has an average crystallite size of ~31 nm, matches the International Centre for Diffraction Data powder diffraction file (PDF) #034-0189 and contains trace (<2 wt %) periclase (MgO, PDF #045-0946).

In Operando X-ray Diffraction

Time-resolved XRD experiments were conducted at 90 °C and 65 °C at 90±1 bar in a pressurized static reactor with a beryllium cap. The *in operando* X-ray diffraction (XRD) experimental apparatus has been described in detail [1, 3-5]. For all the experiments, 10 µl of deionized distilled (DDI) water was placed in the reactor. This mass of water ensured that the CO_2 was always fully saturated with respect to water, based on the mutual solubility CO_2-H_2O model of Spycher et al. [6] and the sensitivity analysis of Miller et al. [1]

specific to the *in operando* XRD reactor. The forsterite powder (4.5 mg) was lightly packed into the XRD sample holder that was not in contact with the solution reservoir below.

The *in operando* XRD reactor was housed in an X-ray diffractometer capable of analyzing crystalline phase evolution at elevated pressure and temperatures. The diffractometer scanned the sample every 210 seconds; area detector images and background-subtracted intensity vs. °2θ diffractograms were visually examined to detect any transitory phases (Figure S1 and Figure S2). Quantitative analysis of selected time-resolved patterns at ~2 hour intervals allowed the evolving phase abundances of the carbonating sample to be determined with estimated uncertainties of ±5 wt % [1-2]. Reproducibility was demonstrated by replicate *in operando* XRD experiments in Miller et al. [1-2] and this work (two 90 °C experiments). Additional information about the quantitative *in operando* XRD analysis methods, including sample loading, reactor pressurization, data acquisition, pattern refinement procedures, and determination of uncertainties can be found in Miller et al. [1-2].

Carbonation Kinetics Calculations

Phase abundances determined from refinements of time-resolved *in operando* XRD patterns were corrected to account for amorphous silica and facilitate direct comparisons with TGA-MS results. Quantitative *in operando* XRD results are reported in wt % relative to the total amount of crystalline material, as amorphous phases were not detectable or quantifiable in this study. We assumed that the forsterite carbonation reactions proceeded in accordance with the stoichiometry of Reaction 1 which enabled us to calculate amorphous phase-corrected wt %. The initial mass of forsterite in the experiments was then used to calculate absolute phase abundances in moles. The uncertainty for the mole abundances was estimated to be ±10% of the initial moles of forsterite and is consistent with the ±5 wt % XRD uncertainty, as described in Miller et al. [1-2].

Kinetic models were fit to the time series of calculated mole abundances from this study and from the 50 °C and 90 bar forsterite carbonation dataset from Miller et al. [2]. The 50 °C rate constant from that study was determined after an extended ~20 hr induction time, due to citrate inhibiting nucleation, was removed [2]. The mineral abundance results were successfully fit in SigmaPlot 12.5 (Systat Software Inc.) to exponential rise to maximum expressions:

$$Q_t=a(1-e^{-kt}) \quad (2)$$

where Q_t is the amount (moles) of magnesite at time t (seconds), a is a constant, and k is k_{Mgs}, the magnesite precipitation rate constant (s^{-1}). The uncertainty of the rate constant, as calculated in SigmaPlot 12.5, ranged from 12-23%. The rate constants from the four 50-90 °C experiments were then used to calculate the apparent activation energy (E_a) of nanoconfined magnesite precipitation using the Arrhenius relationship given by:

$$k = A_a e^{\frac{-E_a}{RT}} \quad (3)$$

where R is the gas constant, T is the absolute temperature, and A_a designates a pre-exponential factor. Magnesite precipitation rate constants were plotted on an Arrhenius plot with the 50 °C and 90 bar forsterite carbonation rate constant from Miller et al. [2]. The Arrhenius plot depicts the natural logarithm of the rate constants as a function of 1000 times the inverse absolute temperature. Lines of best fit were determined with simple linear regression and the negative slopes divided by R resulted in the apparent activation energy of forsterite carbonation in kJ/mol. The activation energy has a conservative uncertainty of ±17% (6 kJ/mol), three times the propagated uncertainty of the Arrhenius plot slope. The activation energy is an apparent activation energy because it describes the complex series of all elementary reactions

that compose the mineral dissolution and precipitation reactions of forsterite to magnesite carbonation reaction. The number of rates (four) and temperatures (three) used to calculate the activation energy is standard for carbonate precipitation studies [7-12].

Lastly, in order to evaluate the relationship between k_{Mgs} and Mg^{2+} dehydration kinetics, we calculated the water exchange rates around an aqueous magnesium ion at 50, 65, and 90 °C using the procedures previously described in Bracco et al. [13]. Briefly, we parametrized the Eyring equation [14] with the enthalpy (42.6 kJ/mol) and entropy (8.4 J mol^{-1} K^{-1}) of activation [15] to extrapolate the room temperature water exchange rate (k_{H2O}) to our experimental conditions. Our experimentally-determined k_{Mgs} results correlate exceptionally well (R^2>0.99) with calculated water exchange rates around aqueous magnesium cations (Figure S4), and this supports the idea that magnesite growth rates are limited by the dehydration of magnesium cations prior to incorporation into the magnesite lattice. This correlation is consistent with the idea that ligand exchange reactions control rates of mineral dissolution [16-17] and growth [18].

Ex Situ Characterization

Upon completion of magnesite precipitation experiments, reacted powders were removed from the sample holder and analyzed using thermogravimetric analysis coupled to mass spectrometry (TGA-MS) to complement and validate the *in operando* XRD results. [1-2] Sample weight changes during thermal decomposition were measured with a precision microbalance and associated CO_2 and H_2O releases were observed through changes in ion currents (*m/z*) of mass 44 and 18, respectively (Figure S4). The mass loss between 200 °C and 850 °C was used to calculate the magnesite abundance (±5 wt %) in the sample. This temperature range was chosen to quantify the weight loss due to CO_2. These ex situ analyses determined the extent of carbonation and confirmed that no hydrated phases were present.

SI Tables

Magnesite ($MgCO_3$) precipitation apparent activation energies Mean=103.0, median=93.3, n=7, SD=26.6		
Activation Energy (kJ/mol)	*Temperature (°C)*	*Reference*
159	90-100	Saldi, et al. [7]
122.6[a]	120-180	Di Lorenzo, et al. [11]
100[a]	110-200	Zhang, et al. [19]
93.3[a]	120-180	Di Lorenzo, et al. [11]
85.1	100-146	Gautier, et al. [9]
81[a]	110-200	Zhang, et al. [19]
80.2	100-200	Saldi, et al. [8]
Calcite ($CaCO_3$) precipitation activation energies Mean=44.2, median=45.4, n=10, SD=3.3		
Activation Energy (kJ/mol)	*Temperature (°C)*	*Reference*
48.1	10-40	Inskeep and Bloom [20]
46.9	25-90	Nagy [21]
45.8	5-30	Cassford, et al. [22]
46.0	10-40	Nancollas and Reddy [23]
46	20-70	Gutjahr, et al. [24]
45	15-35	Takasaki, et al. [25]
44.8	10-50	Dromgoole and Walter [26]
43.1	10-40	Wiechers, et al. [27]
39.3[b]	15-35	Kazmierczak, et al. [28]
37.2	10-50	Dromgoole and Walter [26]
SD, standard deviation [a] In these studies, the activation energy is for the solution-mediated transformation reaction of hydromagnesite [$(Mg_5(CO_3)_4(OH)_2 \cdot 4H_2O$] to magnesite. [b] Arvidson and Mackenzie [29] used the approach of Lippmann [30] in conjunction with the calcite activation energy of Kazmierczak, et al. [28] to calculate a magnesite precipitation activation energy of 92.9 kJ/mol.		

Table S1. Compiled apparent activation energies for magnesite and calcite precipitation.

Temperature[a] (°C)	Pressure (bar)	Reaction time (hrs.)	k_{H_2O}, calculated water exchange rate of Mg^{2+} (s^{-1})	*in operando* XRD crystalline phase abundance[b] (wt %)		Corrected *in operando* XRD magnesite abundance[b] (wt %)	k_{Mgs}, magnesite precipitation rate constant (s^{-1})
				Forsterite	Magnesite		
90	90	23.0	$1.5x10^{7}$	3	97	72	$2.9x10^{-5}$±14%
90	90	24.9	$1.5x10^{7}$	4	96	71	$2.6x10^{-5}$±12%
65	91	45.0	$4.9x10^{6}$	13	87	67	$1.1x10^{-5}$±23%
50[c]	90	71.5[d]	$2.3x10^{6}$	10	90	68	$6.5x10^{-6}$±12%

Table S2. Experimental parameters and results.

Abbreviations: XRD - X-ray diffraction; TGA-MS - thermogravimetric mass spectrometry

[a] All of the experiments were conducted with 10 µl of DDI water in the reactor fluid reservoir. The *in operando* XRD reactor contained 0.45 g of CO_2 at 90 °C bar and 0.55 g of CO_2 at 65 °C.

[b] ±5 wt % uncertainty

[c] This 50 °C and 90 bar experiment is from Miller et al. [2] and was used in this study to calculate a rate constant for magnesite precipitation.

[d] As described in Miller et al. [2] the reaction time and precipitation rate constant was calculated after removing a ~20 hr induction (nucleation) time.

SI Figures

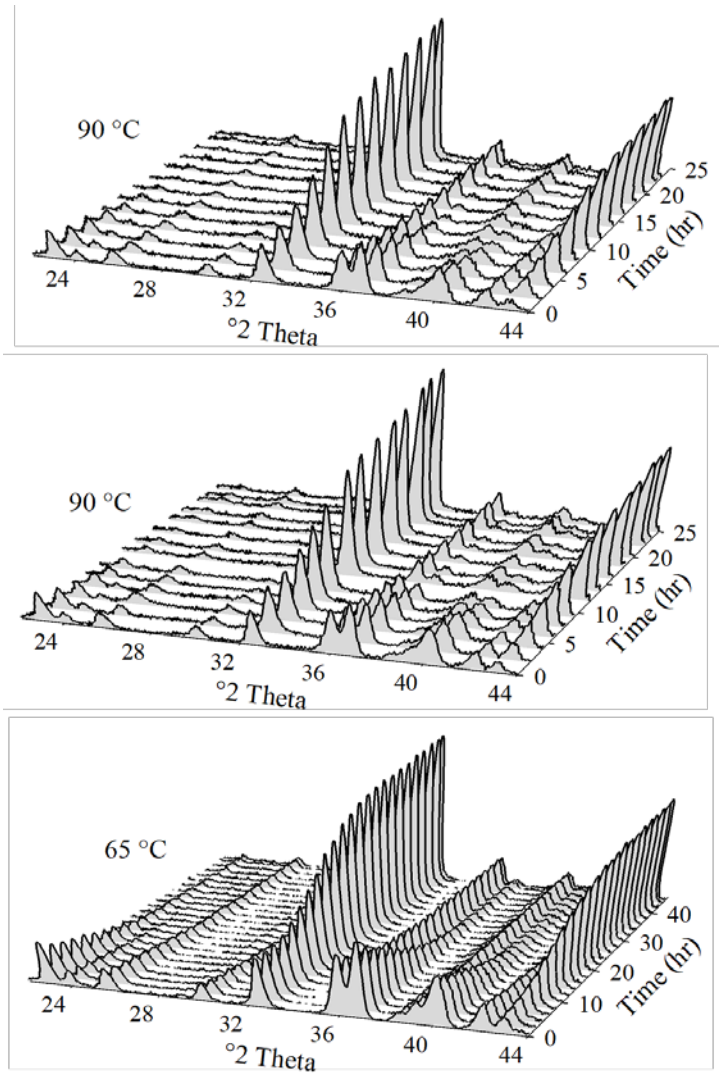

Figure S1. Time-resolved diffractograms for the three *in operando* experiments.

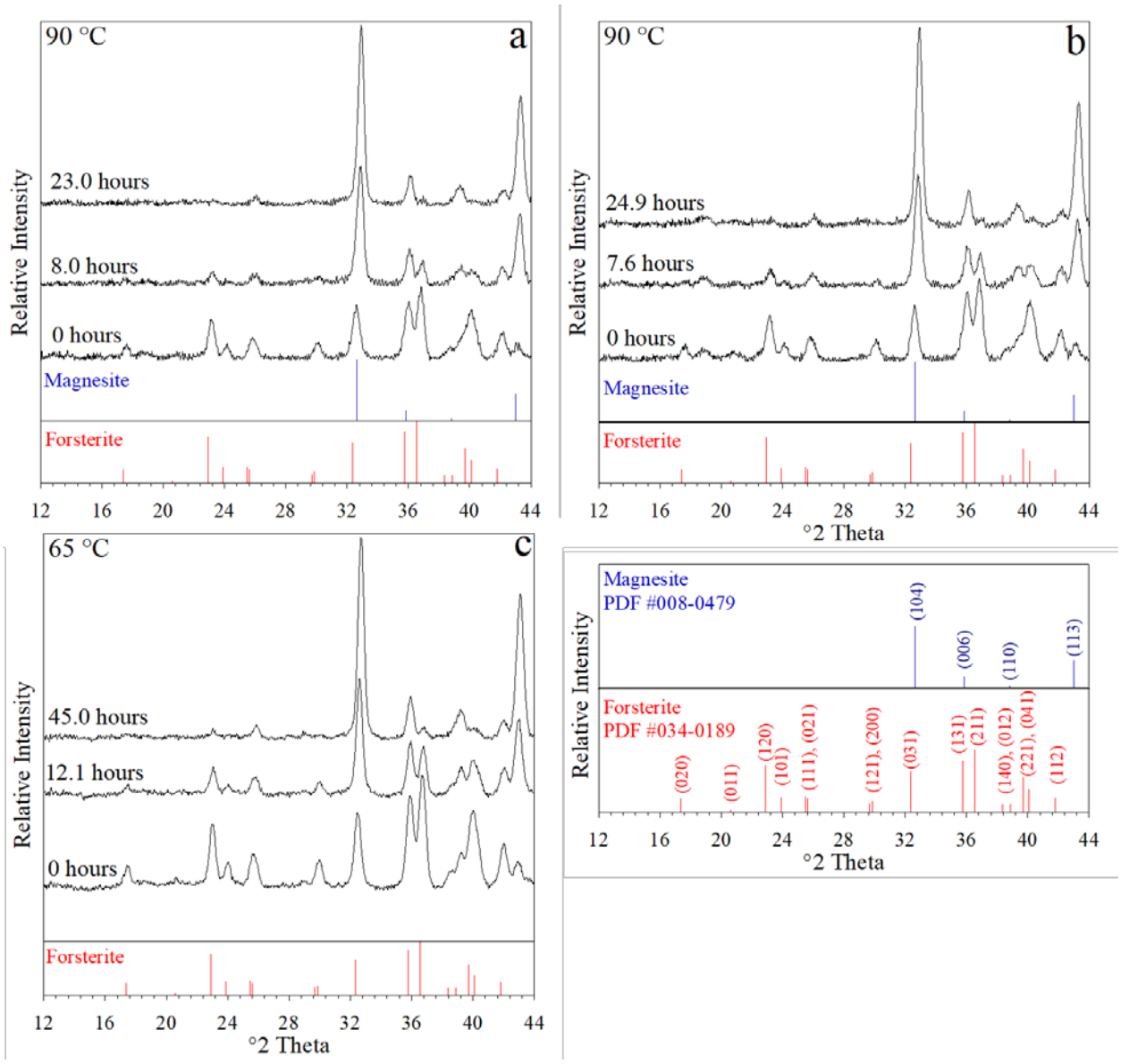

Figure S2: Selected diffractograms from *in operando* XRD experiments with powder diffraction file reference lines for forsterite and magnesite. The additional panel specifies the Miller Indices for the powder diffraction file (PDF) reference lines. Where space is limited, the designations are stacked and separated by a comma.

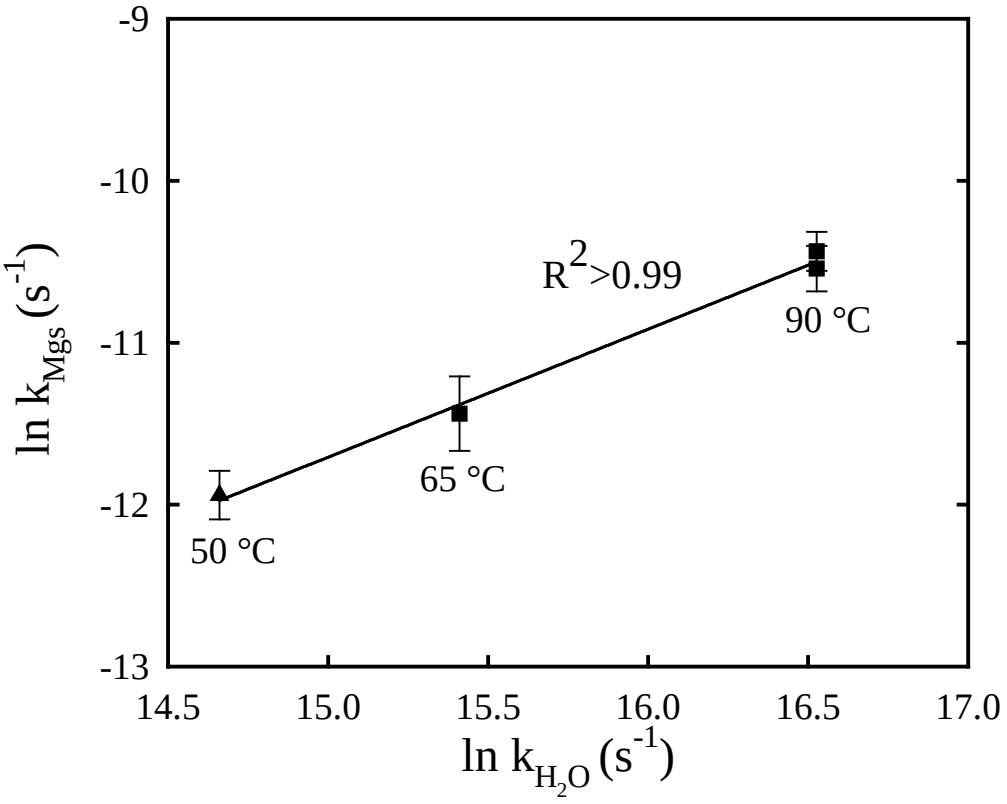

Figure S3. Correlated magnesite precipitation rate constant (k_{Mgs}) and the calculated water exchange rate (k_{H2O}) around Mg^{2+}(aq) ions. See SI text above for more details.

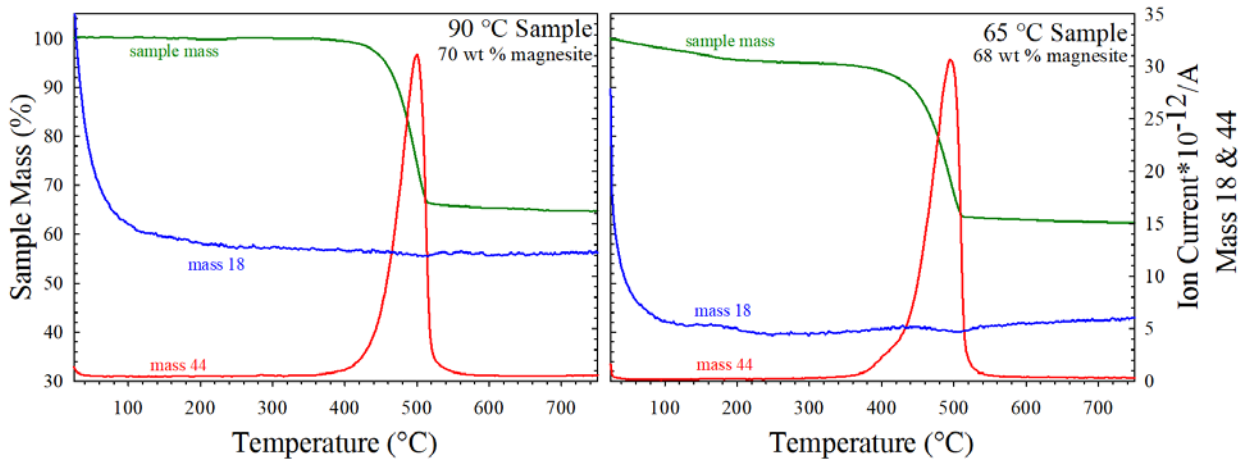

Figure S4. Thermogravimetric mass spectrometry results that confirm the XRD-determined carbonation extents presented in Table S2.

SI References

(1) Miller, Q. R. S.; Kaszuba, J. P.; Schaef, H. T.; Bowden, M. E.; McGrail, B. P. Impacts of Organic Ligands on Forsterite Reactivity in Supercritical Co_2 Fluids. *Environ. Sci. Technol.* **2015,** *49* (7), 4724-4734, DOI: 10.1021/es506065d.

(2) Miller, Q. R. S.; Schaef, H. T.; Kaszuba, J. P.; Qiu, L.; Bowden, M. E.; McGrail, B. P. Tunable Manipulation of Mineral Carbonation Kinetics in Nanoscale Water Films Via Citrate Additives. *Environ. Sci. Technol.* **2018,** *52* (12), 7138-7148, DOI: 10.1021/acs.est.8b00438.

(3) Schaef, H. T.; McGrail, B. P.; Loring, J. L.; Bowden, M. E.; Arey, B. W.; Rosso, K. M. Forsterite [Mg_2sio_4] Carbonation in Wet Supercritical Co_2: An in Situ High Pressure X-Ray Diffraction Study. *Environ. Sci. Technol.* **2013,** *47* (1), 174-181, DOI: 10.1021/es301126f.

(4) Schaef, H. T.; Windisch, C. F., Jr.; McGrail, B. P.; Martin, P. F.; Rosso, K. M. Brucite [$Mg(Oh)_2$] Carbonation in Wet Supercritical Co_2: An in Situ High Pressure X-Ray Diffraction Study. *Geochim. Cosmochim. Acta* **2011,** *75* (23), 7458-7471, DOI: 10.1016/j.gca.2011.09.029.

(5) Miller, Q. R. S.; Thompson, C. J.; Loring, J. S.; Windisch, C. F.; Bowden, M. E.; Hoyt, D. W.; Hu, J. Z.; Arey, B. W.; Rosso, K. M.; Schaef, H. T. Insights into Silicate Carbonation Processes in Water-Bearing Supercritical Co_2 Fluids. *Int. J. Greenhouse Gas Control* **2013,** *15*, 104-118, DOI: 10.1016/j.ijggc.2013.02.005.

(6) Spycher, N.; Pruess, K.; Ennis-King, J. Co_2-H_2o Mixtures in the Geological Sequestration of Co_2. I. Assessment and Calculation of Mutual Solubilities from 12 to 100°C and up to 600 Bar. *Geochim. Cosmochim. Acta* **2003,** *67* (16), 3015-3031, DOI: 10.1016/s0016-7037(03)00273-4.

(7) Saldi, G. D.; Jordan, G.; Schott, J.; Oelkers, E. H. Magnesite Growth Rates as a Function of Temperature and Saturation State. *Geochim. Cosmochim. Acta* **2009,** *73* (19), 5646-5657, DOI: 10.1016/j.gca.2009.06.035.

(8) Saldi, G. D.; Schott, J.; Pokrovsky, O. S.; Gautier, Q.; Oelkers, E. H. An Experimental Study of Magnesite Precipitation Rates at Neutral to Alkaline Conditions and 100-200 °C as a Function of Ph, Aqueous Solution Composition and Chemical Affinity. *Geochim. Cosmochim. Acta* **2012,** *83*, 93-109, DOI: 10.1016/j.gca.2011.12.005.

(9) Gautier, Q.; Benezeth, P.; Schott, J. Magnesite Growth Inhibition by Organic Ligands: An Experimental Study at 100, 120 and 146 °C. *Geochim. Cosmochim. Acta* **2016,** *181*, 101-125, DOI: 10.1016/j.gca.2016.02.028.

(10) Gautier, Q.; Bénézeth, P.; Mavromatis, V.; Schott, J. Hydromagnesite Solubility Product and Growth Kinetics in Aqueous Solution from 25 to 75 °C. *Geochim. Cosmochim. Acta* **2014,** *138*, 1-20.

(11) Di Lorenzo, F.; Rodriguez-Galan, R. M.; Prieto, M. Kinetics of the Solvent-Mediated Transformation of Hydromagnesite into Magnesite at Different Temperatures. *Min. Mag.* **2014,** *78* (6), 1363-1372, DOI: 10.1180/minmag.2014.078.6.02.

(12) Whitfield, P. S.; Mitchell, L. D. In Situ Laboratory X-Ray Powder Diffraction Study of Wollastonite Carbonation Using a High-Pressure Stage. *Appl. Geochem.* **2009,** *24* (9), 1635-1639, DOI: 10.1016/j.apgeochem.2009.04.030.

(13) Bracco, J. N.; Stack, A. G.; Higgins, S. R. Magnesite Growth Rates as a Function of the Aqueous Magnesium-to-Carbonate Ratio. *Cryst. Growth Des.* **2014,** *247*.

(14) Eyring, H. The Activated Complex and the Absolute Rate of Chemical Reactions. *Chem. Rev.* **1935,** *17* (1), 65-77.

(15) Neely, J.; Connick, R. Rate of Water Exchange from Hydrated Magnesium Ion. *J. Am. Chem. Soc.* **1970,** *92* (11), 3476-3478.

(16) Casey, W. H.; Westrich, H. R. Control of Dissolution Rates of Orthosilicate Minerals by Divalent Metal–Oxygen Bonds. *Nature* **1992,** *355*, 157, DOI: 10.1038/355157a0.

(17) Pokrovsky, O.; Schott, J. Surface Chemistry and Dissolution Kinetics of Divalent Metal Carbonates. *Environ. Sci. Technol.* **2002,** *36* (3), 426-432.

(18) Stack, A. G.; Grantham, M. C. Growth Rate of Calcite Steps as a Function of Aqueous Calcium-to-Carbonate Ratio: Independent Attachment and Detachment of Calcium and Carbonate Ions. *Cryst. Growth Des.* **2010,** *10* (3), 1409-1413, DOI: 10.1021/cg901395z.

(19) Zhang, P.; Anderson, H. L.; Kelly, J. W.; Krumhansl, J. L.; Papenguth, H. W. *Kinetics and Mechanisms of Formation of Magnesite from Hydromagnesite in Brine, Technical Report San099-19465*; Sandia National Labs., Albuquerque, NM (US); Sandia National Labs., Livermore, CA (US): 2000.

(20) Inskeep, W. P.; Bloom, P. R. An Evaluation of Rate Equations for Calcite Precipitation Kinetics at Pco_2 Less Than 0.01 Atm and Ph Greater Than 8. *Geochim. Cosmochim. Acta* **1985,** *49* (10), 2165-2180.

(21) Nagy, K. L. The Solubility of Calcite in Nacl and Na-Ca-Cl Brines. *PhD Dissertation* **1988,** *Texas A&M University*.

(22) Cassford, G. E.; House, W. A.; Pethybridge, A. D. Crystallisation Kinetics of Calcite from Calcium Bicarbonate Solutions between 278.15 and 303.15 K. *J. Chem. Soc. Faraday Trans. 1* **1983,** *79* (7), 1617-1632.

(23) Nancollas, G. H.; Reddy, M. M. Crystallization of Calcium Carbonate Ii. Calcite Growth Mechanism. *J. Colloid Interface Sci.* **1971,** *37* (4), 824-830, DOI: 10.1016/0021-9797(71)90363-8.

(24) Gutjahr, A.; Dabringhaus, H.; Lacmann, R. Studies of the Growth and Dissolution Kinetics of the $Caco_3$ Polymorphs Calcite and Aragonite I. Growth and Dissolution Rates in Water. *J. Cryst. Growth* **1996,** *158* (3), 296-309.

(25) Takasaki, S.; Parsiegla, K. I.; Katz, J. L. Calcite Growth and the Inhibiting Effect of Iron (Iii). *J. Cryst. Growth* **1994,** *143* (3-4), 261-268.

(26) Dromgoole, E. L.; Walter, L. M. Inhibition of Calcite Growth Rates by Mn^{2+} in $Cacl_2$ Solutions at 10, 25, and 50°C. *Geochim. Cosmochim. Acta* **1990,** *54* (11), 2991-3000.

(27) Wiechers, H. N. S.; Sturrock, P.; Marais, G. V. R. Calcium Carbonate Crystallization Kinetics. *Water Res.* **1975,** *9* (9), 835-845.

(28) Kazmierczak, T. F.; Tomson, M. B.; Nancollas, G. H. Crystal Growth of Calcium Carbonate. A Controlled Composition Kinetic Study. *J. Phys. Chem.* **1982,** *86* (1), 103-107.

(29) Arvidson, R. S.; Mackenzie, F. T. Temperature Dependence of Mineral Precipitation Rates Along the $Caco_3$-$Mgco_3$ Join. *Aquat. Geochem.* **2000,** *6* (2), 249-256, DOI: 10.1023/a:1009619426406.

(30) Lippmann, F. *Sedimentary Carbonate Minerals*, Springer Berlin Heidelberg: Berlin, Heidelberg, 1973; Vol. 6, p 228.